Extraction process optimization of alisol B 23-acetate from Alismatis Rhizoma and its protection against carbon tetrachloride-induced acute liver injury ☆

Peng Lei [a], Zhirong Zhou [a], Jierong Pei [a], Li Jia [a], Lifeng Han [a,b], Miaomiao Jiang [a,b,*]

[a] Tianjin Key Laboratory of Therapeutic Substance of Traditional Chinese Medicine, Tianjin, China
[b] Haihe Laboratory of Modern Chinese Medicine, Tianjin, China

ABSTRACT

Alisol B 23-acetate (AB23A) is an important pharmacodynamic compound found in Alismatis Rhizoma. In this study, response surface methodology (RSM) and Box- Behnken design (BBD) were used to optimize the extraction parameters of the AB23A. The optimal conditions included a solid–liquid ratio of 1:13, a reflux extraction of 70% ethanol, an extraction time of 2 h, and an extraction cycle of 3 cycles. Furthermore, a rat model of acute liver injury was established using carbon tetrachloride (CCl_4), and a comprehensive analysis combining histopathology, lipidomics, and metabolomics was conducted to elucidate the hepatoprotective effect of AB23A. The findings revealed that AB23A significantly reduced the levels of serum aspartate aminotransferase (AST), alanine aminotransferase (ALT), and alkaline phosphatase (ALP), and restored the abnormal morphology of hepatocytes. Furthermore, AB23A exhibited the ability to attenuate CCl_4-induced lipid peroxidation, as evidenced by the upregulation of glutathione (GSH) and glutathione peroxidase 4 (GPX4) levels, along with a reduction in malondialdehyde (MDA) content in the liver. Omics results and immunohistochemistry analyses demonstrated a decrease in inflammatory reaction and oxidized phospholipid levels following AB23A administration, indicating an enhanced anti-inflammatory and antioxidant capacities of hepatocytes. Differential metabolite analysis revealed that AB23A improved anti-inflammatory and antioxidant capacities by modulating liver sphingolipid metabolism and purine metabolism, thereby enhancing hepatocyte recovery and counteracting acute liver injury induced by CCl_4.

1. Introduction

Carbon tetrachloride (CCl_4) is a typical hepatotoxic substance that is widely used in industrial production, such as insecticide, detergent, extractant, fire extinguishing agent and analytical reagent (Cohen et al., 2023). When the high concentration of CCl_4 vapor or solution is introduced into the body, this toxic compound becomes enriched and metabolized within the liver. Metabolism is primarily facilitated by cytochrome P450 enzymes, resulting in the formation of trichloromethyl radical (CCl_3) and trichloromethylperoxy radical (CCl_3O_2) (W. Wang et al., 2023; Unsal et al., 2021; Heimberg and Weinstein, 1962). These radicals have the propensity to attack phospholipid molecules within the cellular membrane system, leading to lipid peroxidation. Additionally, they can covalently bind to membrane lipids and protein macromolecules, thereby destroying membrane structure and function (Watts, 1950; Xue et al., 2022). Consequently, this process disrupts liver metabolism, giving rise to lipid peroxidation, inflammation, and oxidative stress. It is vital to search for drugs that can regulate liver metabolism and alleviate the harm caused by CCl_4.

From ancient times to the present, medicinal plants have played an

increasingly important role in safeguarding human health (Fernández et al., 2021; Ferrarini et al., 2022; Meng et al., 2022; Şahin et al., 2023; Yang et al., 2022). Exploring active ingredients from natural products has become a crucial avenue for the development of new drugs (Bai et al., 2022; He et al., 2023; Qu et al., 2023). Alismatis Rhizoma is the dried rhizomes of the plants *Alisma orientale* (Sam.) Juzep. or *Alisma plantago-aquatica* Linn. and has been used to protect the liver and kidney since ancient times. Alisol B 23-acetate (AB23A, Fig. 1A), a prominent constituent of Alismatis rhizome, exhibits a diverse range of pharmacological activities, including lipid reduction (Wu et al., 2023; Fu et al., 2022), anti-tumor (Chen et al., 2022; Ye et al., 2022), anti-allergic (Shao et al., 2018), and intestinal protection (Xia et al., 2022; Zhu et al., 2021). Considering the broad application prospects of AB23A, it is essential to optimize its extraction conditions to efficiently obtain the target compound from the Alismatis rhizome. In addition, our previous study demonstrated the beneficial effects of Alismatis Rhizoma in ameliorating metabolic syndrome induced by high fructose consumption (Jia et al., 2022). However, the impact of AB23A on CCl_4-induced liver lipid peroxidation, oxidative stress, and metabolic dysregulation remains unclear.

The objective of this study was to optimize the extraction process of AB23A, and elucidate the protective effects of AB23A against acute liver injury induced by CCl_4 by investigate the influence of AB23A on alterations in liver lipid profiling and metabolic dysfunction resulting from CCl_4-induced liver injury.

2. Materials and methods

2.1. Materials

Carbon tetrachloride (CCl_4, purity > 98 %) was purchased from Macklin Inc. (Shanghai, China). AB23A (HPLC ≥ 98 %, batch number: RFS- Y03601906010) was purchased from Chengdu Herbpurify Co., Ltd. (Chengdu, China). Bifendatatum (purity > 97 %, batch number: C1904020) was purchased from Shanghai Aladdin Biochemical Technology Co., Ltd. (Shanghai, China). E06 mouse monoclonal antibody was purchased from Avanti Polar Lipids, Inc. (Alabama, USA). Goat anti-mouse IgM / HRP antibody was purchased from Beijing Biosynthesis Biotechnology Co., Ltd. (Beijing, China). Hematoxylin staining solution and Eosin staining solution were provided by Wuhan Servicebio Technology Co., Ltd. (Wuhan, China). Assay kits for aspartate aminotransferase (AST), alanine aminotransferase (ALT), alkaline phosphatase (ALP), glutathione (GSH) and malondialdehyde (MDA) were purchased from Nanjing Jiancheng Biological Engineering Research Institute (Nanjing, China). Enzyme-linked immunosorbent assay (ELISA) kits for glutathione peroxidase 4 (GPX4) was obtained from ZCIBIO Technology Co., Ltd (Shanghai, China).

2.2. Extraction of AB23A

Alismatis Rhizoma was provided and identified by Beijing Tongrentang Tianjin Nankai Pharmacy Co., Ltd (Tianjin, China). The samples were kept in the State Key Laboratory of Component-based Chinese Medicine. Extraction of AB23A from the powdered medicinal herb was performed using the reflux extraction method. The Alismatis Rhizoma powder (passed through a No. 5 sieve) was weighed at 1 g and reflux-extracted with 10 mL of 95 % ethanol for 1 h. After reflux extraction, the reduced weight was compensated with additional extraction solvent. Then the extract was diluted 5 times and centrifuged at $20,000 \times g$ for 5 min. The supernatant was collected to obtain the test sample solution. AB23A reference standard was dissolved in methanol to prepare a reference solution with a concentration of 128 µg/mL. The determination method for the content of AB23A in the sample was established using the test sample solution and the reference solution.

Based on the aforementioned method for preparing the test sample solution, a single-factor experiment was employed to optimize the extraction efficiency of AB23A by varying the following parameters: ethanol concentration (50 %, 60 %, 70 %, 80 %, 95 %), solid–liquid ratio (1:6, 1:8, 1:10, 1:12, 1:15), extraction time (1 h, 1.5 h, 2 h, 2.5 h, 3 h), and extraction cycles (1, 2, 3, 4, 5). The extracted solution was then subjected to centrifugation at $20,000 \times g$ for 5 min, and the supernatant was collected for analysis using ultra performance liquid chromatography (UPLC).

2.3. Ultra performance liquid chromatography analyses of samples

Samples were analyzed using the ACQUITY UPLC H-Class PLUS system (Waters, USA) equipped with an ACQUITY UPLC BEH C18 column (2.1 × 50 mm, 1.7 µm, Waters, USA). 3 µL of the sample was injected into the system, and then eluted through the chromatographic column at a flow rate of 0.3 mL/min while the column temperature was set at 35 °C. The chemical components in the sample were detected at a wavelength of 208 nm. The separation was achieved using a gradient elution method with water and acetonitrile as mobile phases A and B, respectively. The gradient elution program was as follows: 0–1 min, 30 %-55 % B; 1–3 min, 55 %-70 % B; 3–7 min, 70 % B; 7–8 min, 70 %-90 % B; 8–9 min, 90 %-30 % B; 9–10 min, 30 % B. The development and validation of the AB23A measurement method in the sample were conducted using the AB23A standard substance. The linearity of the method was evaluated by plotting peak areas against standard substance concentrations, and the accuracy of the method for determining AB23A content in the sample was determined by conducting examinations of precision, repeatability, stability, and recovery rate.

2.4. Response surface methodology design

Based on the preliminary single-factor experiments, a four-factor three-level Box-Behnken design (BBD) was conducted. A binary polynomial regression equation for the extraction efficiency of AB23A concerning factors A, B, C, and D was obtained by conducting 29 sets of randomized sequential experiments. Subsequently, response surface plots were generated to analyze the interactions between various factors and determine the optimal extraction process.

2.5. Separation and purification of AB23A

4 kg of Alismatis Rhizoma was pulverized, and extraction was carried out using the optimized method. Combining various chromatographic methods, AB23A was separated, purified, and enriched from the extract, resulting in 3.3 g of monomeric AB23A with a purity of 95.48 % (details are provided in the supplementary materials).

2.6. Animals

All animal maintenance and treatment procedures were conducted in accordance with the Guide for the Care and Use of Laboratory Animals from the National Institutes of Health and were approved by the Committee for Institutional Animal Care and Use at Tianjin University of Traditional Chinese Medicine. Fifty Specific Pathogen Free (SPF) SD rats, weighing 200 ± 20 g, were obtained from Beijing HFK Bioscience Co., Ltd. (Beijing, China). The animals were housed at 23 ± 3 ℃ temperature and 60 ± 10 % humidity with a 12 h light/dark photoperiod. The animals were provided with regular laboratory chow and water.

2.7. Administration

The modeling method and dosage for inducing acute liver injury in rats with CCl_4 were referenced from previous reports with slight modifications (Foroutan et al., 2020; Sheng et al., 2022; Zahira et al., 2023). Animals were allowed 1 week to accommodate and randomly divided into five groups (n = 10): the control group (C, 0.5 % CMC-Na solution), the model group (M, 0.5 % CMC-Na solution), the bifendatatum group

(B, 200 mg/kg), the low-dose AB23A (L, 15 mg/kg) and the high-dose AB23A (H, 30 mg/kg). Intragastric administration was performed daily. On the seventh day, acute liver injury was induced in the M, B, L and H group rats by intraperitoneal injection of 2 mL/kg CCl$_4$ (CCl$_4$ / olive oil volume ratio of 1:1) 6 h before the last dosage. Then the animals were fasted without water restriction. The following day, animals were sacrificed under anesthesia, and blood and liver samples were collected. The experimental design is summarized in Fig. 2A.

2.8. Histopathological assessment and immunohistologic analysis

The liver tissue was rinsed with normal saline, weighed, and photographed. Subsequently, the caudate lobe of the liver was fixed in 4 % paraformaldehyde and embedded in paraffin. Followed by cutting into 5 μm-thick sections, tissue sections were stained with hematoxylin and eosin (H&E) and photographed using an optical microscope (Nikon, Japan). Immunohistochemical analysis was conducted on liver tissue sections using E06 IgM to detect oxidized phospholipids (OxPLs). Endogenous peroxidase was blocked with hydrogen peroxide, and nonspecific binding sites were blocked using serum. The primary and secondary antibodies were incubated successively, and the nucleus was finally counterstained with hematoxylin.

2.9. Biochemical assays

Fresh blood samples were centrifuged at $1,400 \times g$ for 10 min at 4 °C, and the resulting supernatant was collected to obtain serum for the analysis of ALT, AST, and ALP. The liver tissue was homogenized at $10,000 \times g$ for 10 min at 4 °C. The supernatant was taken, and the levels of GSH, MDA and GPX4 were measured following the instructions provided by the kit manufacturer.

2.10. Lipidomic analysis

The extraction and analysis of lipids from the liver were performed as we previously reported with slightly modified (Lei et al., 2023). Briefly, 100 mg of liver tissue homogenate was mixed with 1 mL of dichloromethane/methanol (2:1, *V/V*). The sample was thoroughly mixed and then centrifuged. The resulting dichloromethane layer was collected and evaporated using nitrogen gas. The dried sample was reconstituted with 100 μL of isopropanol/methanol (1:1, *V/V*) and centrifuged for detection. Quality control (QC) sample was obtained by mixing 10 μL of each sample.

Liver lipid separation was performed using UltiMate 3000 UHPLC system (Thermo Scientific, USA) equipped with a Hypersil GOLD C18 column (2.1 × 100 mm, 1.9 μm; Thermo Scientific, USA). The column temperature was maintained at 45℃. The mobile phase A consisted of acetonitrile/water (60:40, *V/V*) with 5 mM ammonium formate and 0.1 % formic acid, while mobile phase B comprised acetonitrile/isopropanol (10:90, *V/V*) with 5 mM ammonium formate and 0.1 % formic acid. The following gradient elution was performed at a flow rate of 0.35 mL/min: 0–14.50 min, 40 % − 100 % B; 14.50–16.50 min, 100 % B; 16.50–16.51 min, 100 % − 40 % B; 16.51–20.00 min, 40 % B.

Lipid data were collected using the Q Exactive Orbitrap MS system (Thermo Scientific, USA) connected to UHPLC. HESI − II was performed in positive/negative ionization mode with + 3.5 kV for positive mode and −3.0 kV for negative mode. The MS conditions were as follows: the capillary temperature was 320℃, probe heater temperature was 350℃; sheath gas flow was 35 arb, aux gas flow was 10 arb. Data were acquired in the *m/z* range of 100 − 1500 Da, and product ion scan was acquired using data dependent acquisition (Top N = 5).

2.11. Metabolomic analysis

Metabolites were extracted according to our previous report with appropriate modifications (Lei et al., 2023). 100 mg of liver tissue was homogenized with 500 μL pre-cooled water, followed by the addition of 1 mL of methanol and thorough mixing. The homogenate was subsequently centrifuged at $10,000 \times g$ for 10 min. The supernatant was collected and dried by blowing with nitrogen. The resulting product was redissolved in 100 μL of methanol/water (2:1, *V/V*), and the supernatant was analyzed by UHPLC-MS/MS after centrifugation. 10 μL of each sample was taken and mixed as the QC sample for the determination of instrument stability.

Same as the above analysis conditions of lipidomics, metabolomic analyses were conducted with UltiMate 3000 UHPLC system (Thermo Scientific, USA) coupled with a Q Exactive Orbitrap mass spectrometer (Thermo Scientific, USA). A Waters ACQUITY UPLC HSS T3 column (2.1 × 100 mm, 1.8 μm; Waters, USA) was equipped on the UHPLC-MS/MS system for metabolites separation, and the column was maintained at 45℃ with a flow rate of 0.4 mL/min and the injected volume of each sample was 5.0 μL. The mobile phase was composed of 0.1 % formic acid in distilled water (mobile phase A) and 0.1 % formic acid in methanol (mobile phase B). The applied elution conditions were as follows: 0–2 min, 0.1 % B; 2–6 min, 0.1 % − 25 % B; 6–10 min, 25 % − 80 % B; 10–12 min, 80 % − 90 % B; 12–21 min, 90 % − 99.9 % B; 21–23 min, 99.9 % B; 23–24 min, 99.9 % − 0.1 % B; 24–26 min, 0.1 % B.

Metabolites in samples were detected via Q Exactive Orbitrap mass spectrometer (Thermo Scientific, USA), and the MS parameters were the same as described for lipidomics.

2.12. Data processing and analysis

Lipidomic and metabolomic data were normalized using MS DIAL 4.9 software (Tsugawa et al., 2020) (RIKEN, Japan), and compounds identification was conducted using the built-in database combined with the Human Metabolome Database (HMDB) (Wishart et al., 2022) and previous report (Aoyagi et al., 2017). The multivariate statistical analysis and pathway analysis were carried out by SIMCA (Sartorius, Germany) and MetaboAnalyst (Pang et al., 2021), respectively. Differential lipids and metabolites were screened based on fold change (FC) > 1.5 and $P < 0.05$.

2.13. Statistical analysis

Data were analyzed using GraphPad Prism 9.4 (GraphPad Software, USA) and expressed as mean ± standard deviation. Differences between groups were evaluated by one-way ANOVA followed by the Tukey multiple comparison test. Differences were considered significant at $P < 0.05$.

3. Results

3.1. AB23A extraction process optimization

The chromatograms of the reference standard of AB23A and the extracted liquid sample were shown in Fig. 1B. In the quantitative method for AB23A, the peak area showed a linear relationship with the concentration in the range of 2.00 to 64.0 μg/mL ($y = 8713.1x - 524.72$, $r^2 = 0.9999$). Additionally, the method demonstrated good precision (RSD = 0.51 %), repeatability (RSD = 0.18 %), and stability (RSD = 1.26 %). The average recovery rate was 101.20 % with an RSD of 3.91 %. Therefore, this method could be used for the quantitative analysis of AB23A in the samples.

The results of the single-factor experiments were shown in Fig. 1C. Based on these results, four factors influencing the extraction efficiency of AB23A were identified and encoded as follows: ethanol volume fraction (60 %, 70 %, 80 %) as A, extraction time (1.5 h, 2 h, 2.5 h) as B, extraction cycles (1, 2, 3) as C, and solid–liquid ratio (1:10, 1:12, 1:15) as D. Each factor was assigned three different levels coded as −1, 0, and 1, corresponding to low, medium, and high levels, respectively. These factors were then used in a BBD for optimizing the best process
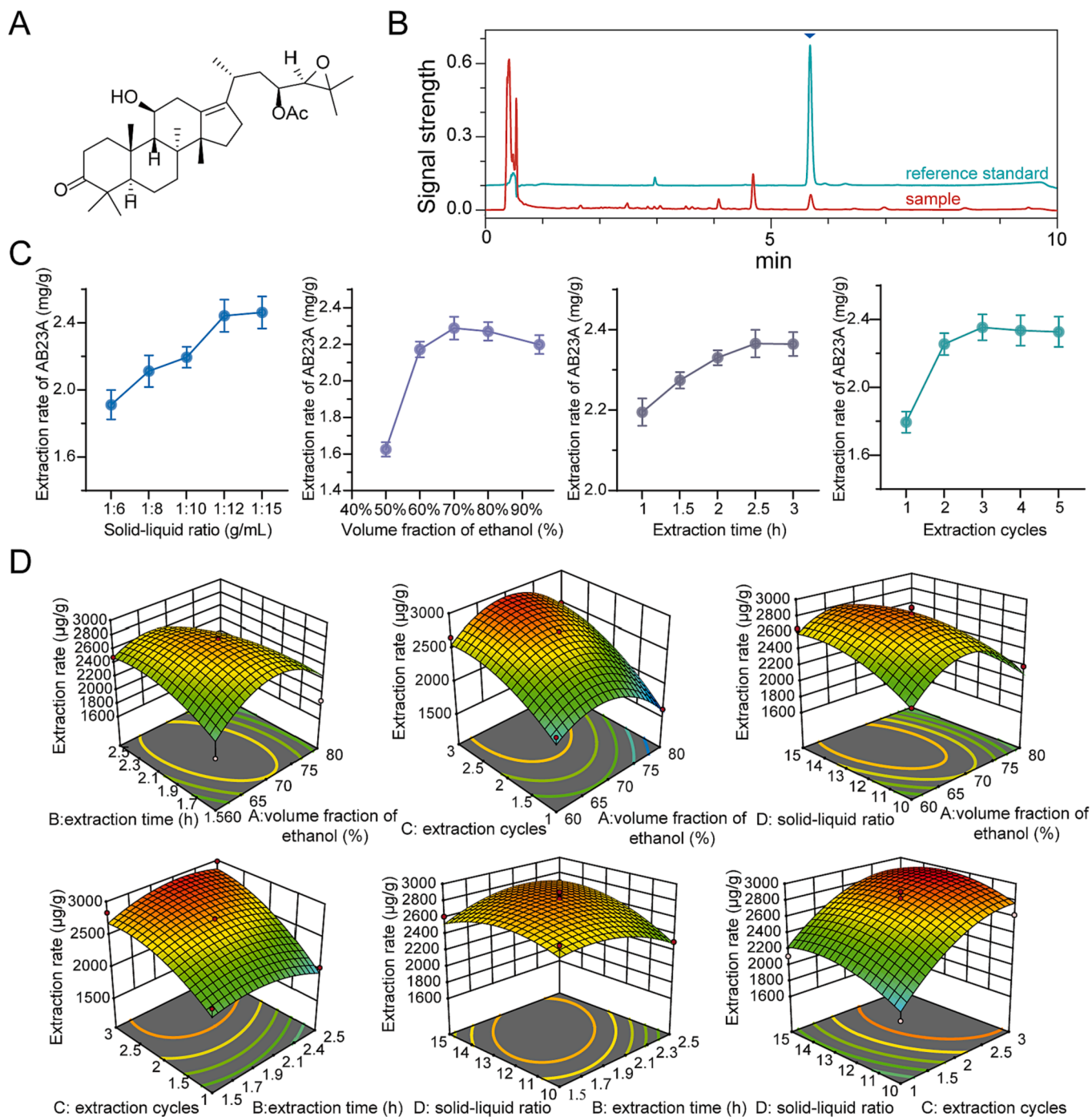
Fig. 1. Structure, chromatograms, and extraction process optimization of Alisol B 23-acetate (AB23A). **(A)** The chemical structure of AB23A. **(B)** Chromatograms of the reference standard of AB23A and sample of AB23A. **(C)** Effect of different solid–liquid ratio, volume fraction of ethanol, extraction time and extraction cycles on the extraction rate of AB23A. **(D)** 3D response surface plots of the interaction of extraction time and volume fraction of ethanol, extraction cycles and volume fraction of ethanol, solid–liquid ratio and volume fraction of ethanol, extraction cycles and extraction time, solid–liquid ratio and extraction time, solid–liquid ratio and extraction cycles on the yield of AB23A.

parameters for AB23A extraction (Table S1). And the binary polynomial regression equation for AB23A extraction efficiency was described by the following equation.

$$
\begin{aligned}
Extraction\ \ rate =\ & 2819.01 - 157.97A - 33.30B + 356.09C + 86.64D \\
& - 181.00AB + 83.37AC - 115.26AD + 98.50BC \\
& + 117.25BD - 42.06CD - 439.64A^2 - 146.47B^2 \\
& - 212.70C^2 - 150.53D^2
\end{aligned}
$$

where A, B, C and D are independent variables in coded form for ethanol volume fraction, extraction time, extraction cycles and solid–liquid ratio, respectively.

The results of the variance analysis for the model were presented in Table S2. The regression equation model showed an F-value of 13.14, with a P-value < 0.0001, indicating that the model was statistically significant. Additionally, the lack-of-fit term had a P-value of 0.1779, suggesting that the lack-of-fit for the model was not significant. The coefficient of determination (r^2) for the model was 0.9293, and the

adjusted R-squared ($r$adj^2) was 0.8586, indicating a high correlation between the predicted values and the actual experimental values. Additionally, based on the F-values and the slopes of the three-dimensional surface plots (Fig. 1D), the interaction effects among factors A, B, C, and D had different effects on the yield of AB23A extraction efficiency, the order was AB > BD > AD > BC > AC > CD, and the order of the impact levels of the single-factor was C > A > D > B.

The data was optimized using Design Expert 12.0 software (Stat-Ease Inc., USA), and the maximum extraction rate of AB23A was found to be 3005.51 μg/g when the ethanol volume fraction was set at 67.29 %, the extraction time was 2.27 h, the extraction cycles were 2.86 times, and the solid–liquid ratio was 1:13.70. Based on practical operational constraints, the optimized extraction process was modified to use a solid–liquid ratio of 1:13 with 70 % ethanol for reflux extraction for 3 cycles,

with each cycle lasting 2 h. The validation experiment was conducted using the modified extraction conditions, and the extraction rate was found to be 2905.82 μg/g, with an RSD of 0.49 %. The close agreement between the experimental results and the predicted values indicated that the extraction process is reliable, and the regression model was reasonable.

3.2. AB23A alleviated acute liver injury caused by carbon tetrachloride

The appearance of the liver was shown in Fig. 2B. Compared with the control group, the liver of the rat treated with CCl₄ exhibited enlargement and whitening, accompanied by a rough and severely damaged surface of the capsule. However, in the bifendatatum and high-dose AB23A groups, the liver surface became smoother, and the color
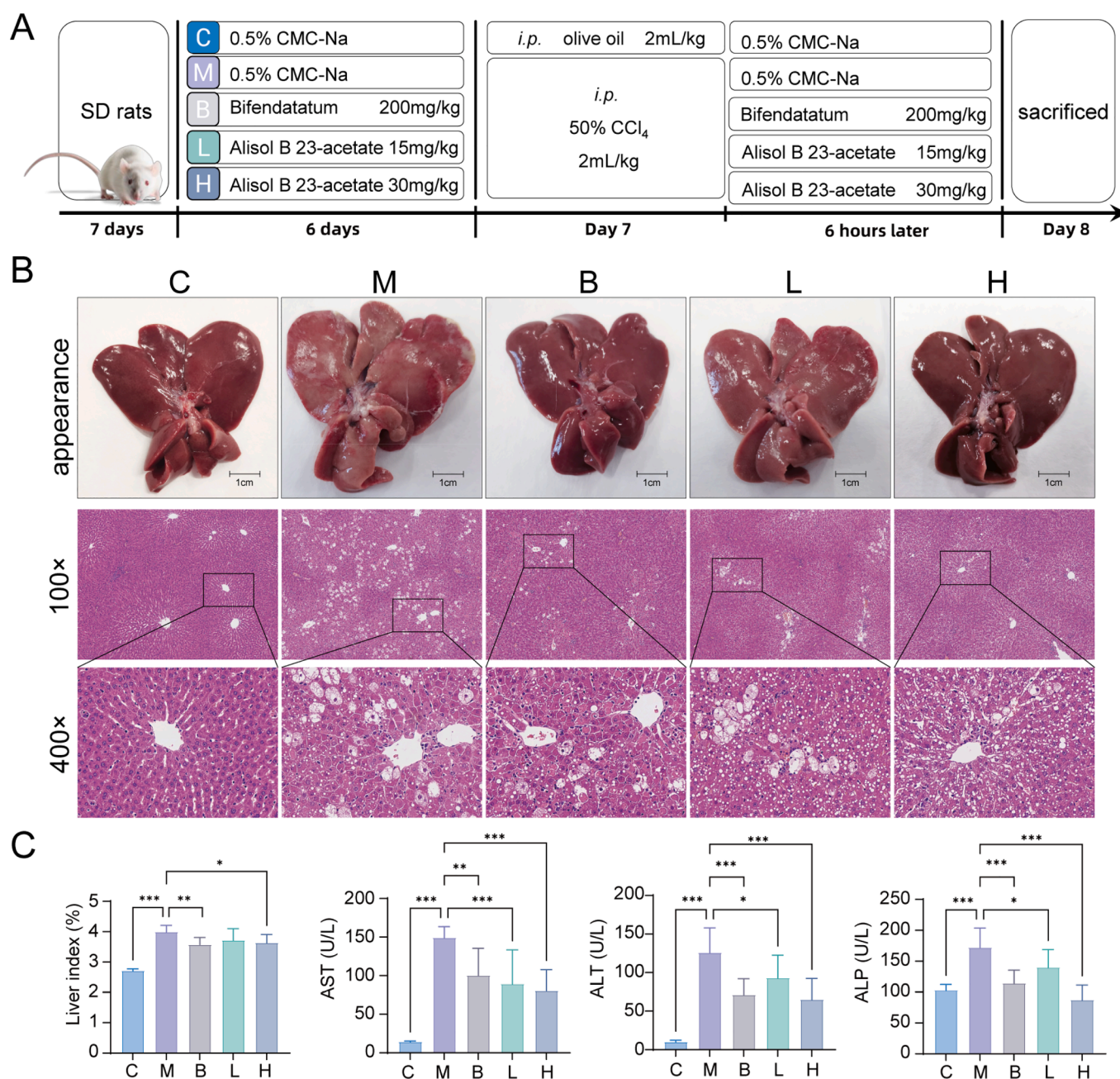
Fig. 2. AB23A could ameliorate acute liver injury induced by CCl₄. **(A)** Experimental groups and treatments. **(B)** Representative appearance photographs of livers and H&E staining of liver sections showed AB23A could maintain hepatocyte morphology and reduce carbon tetrachloride toxicity. **(C)** Liver index evaluation and AST, ALT, ALP levels in serum. *$P < 0.05$, **$P < 0.01$, and ***$P < 0.001$ compared with the model group.

restored to a dark reddish brown, while few areas still showed slight damage to the liver capsule. According to the H&E staining, in the model group, the central vein of the liver was dilated with the surrounding cells necrosis. The hepatocytes appeared enlarged, and ballooning degenerative cells were densely arranged around the central vein. AB23A demonstrated a dose-dependent reduction in lesion damage, maintaining a normal hepatic lobular structure and significantly reducing ballooning degeneration.

The liver index in the model group was markedly increased compared with that in the control group, while AB23A administration could significantly reduce the liver index (Fig. 2C). Additionally, liver conditions were evaluated by analyzing the levels of AST, ALT, and ALP in the serum. As shown in Fig. 2C, CCl_4 treatment led to elevated levels of AST, ALT, and ALP in the serum compared to the control group ($P < 0.05$). Administration of bifendatatum and different doses of AB23A significantly decreased the levels of serum AST, ALT, and ALP ($P < 0.05$), indicating the beneficial effect of AB23A in alleviating CCl_4-induced liver injury.

3.3. AB23A regulated lipid metabolism profiling of the liver

Total ion chromatograms (TIC) of representative samples from various groups in lipidomics were shown in Fig. 3A. Principal component analysis (PCA) was performed to assess the overall differences in
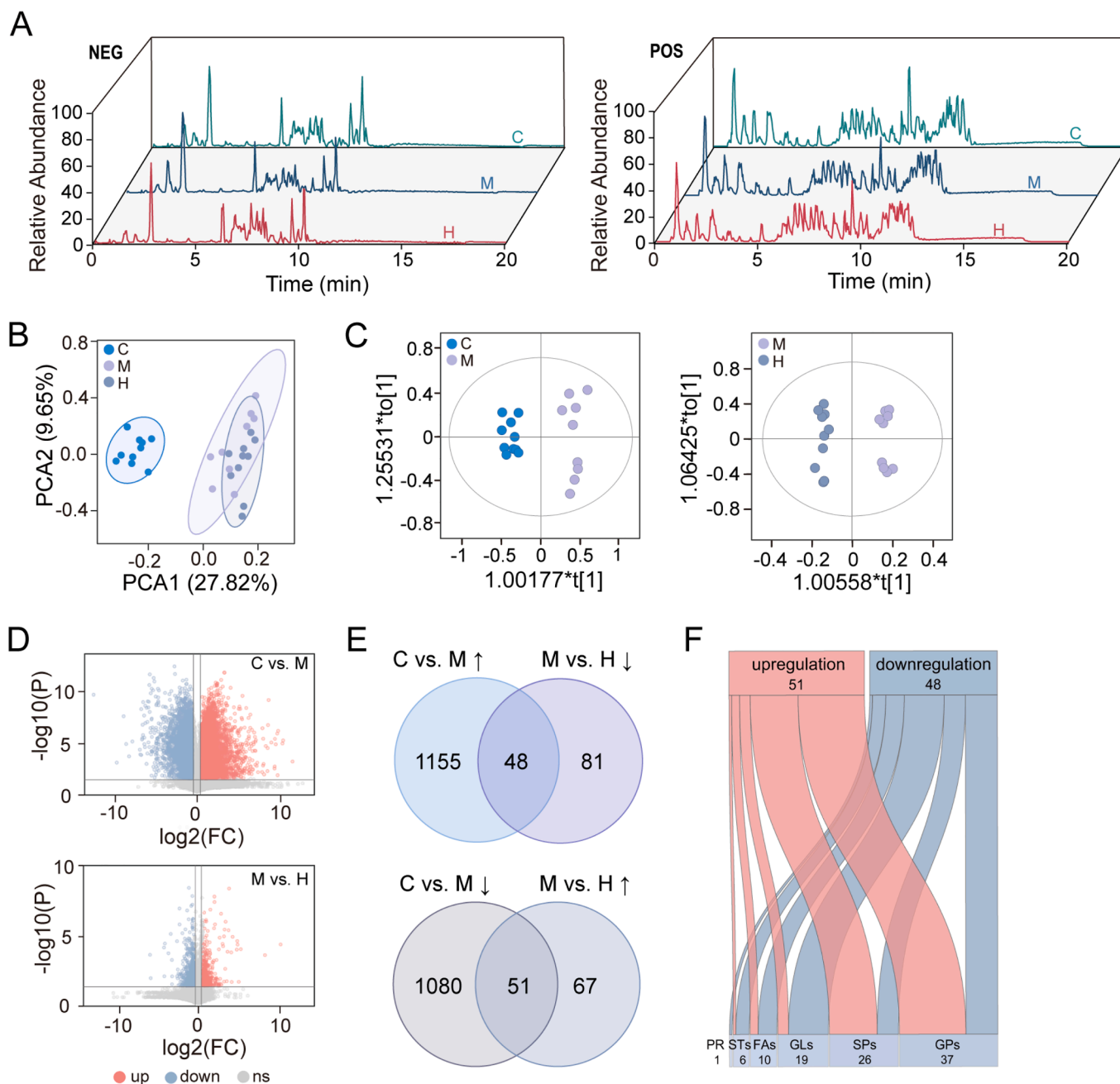
Fig. 3. AB23A mitigated the changes of liver lipid profiling caused by CCl_4. **(A)** Total ion chromatograms of representative samples from various groups in lipidomics in negative and positive ion modes. **(B)** Principal component analysis (PCA) score plot showed the lipid profiling of control (C), model (M), and high dose AB23A administration (H) groups were altered. **(C)** The orthogonal partial least squares-discriminant analysis (OPLS-DA) score plots displayed a clear separation between the two groups (C vs. M, M vs. H). **(D)** The volcano plot analysis showed significantly regulated variables between the two groups ($P < 0.05$, fold change > 1.5). **(E)** The Venn plots demonstrated AB23A could regulate the abnormal lipid caused by CCl_4. **(F)** Lipid category analysis regulated by AB23A.

lipid profiling among the C, M, and H groups (Fig. 3B). And orthogonal projections to latent structures discriminant analysis (OPLS-DA) was used to compare the profiling between C and M groups ($R^2X = 0.557$, $R^2Y = 0.961$, $Q^2 = 0.913$), as well as the M and H groups ($R^2X = 0.426$, $R^2Y = 0.986$, $Q^2 = 0.665$) (Fig. 3C). The results showed that CCl$_4$-induced liver injury led to alterations in the composition of liver lipids, which were ameliorated by AB23A administration. Volcano plots (Fig. 3D) were used to screen the differential variables affected by CCl$_4$ and AB23A intervention. A total of 1203 upregulated and 1131 down-regulated differential lipids were screened and identified in the M group compared to the C group, indicative of the occurrence of acute liver injury induced by carbon tetrachloride. Similarly, 118 upregulated and 129 downregulated differential lipids were identified in the H group compared to the M group. Venn plots (Fig. 3E) were employed to identify the common differential lipids between the C vs. M and M vs. H groups. Among the 1203 lipids upregulated by acute liver injury, AB23A downregulated 48 of them, including 12 glycerophospholipids (GPs), 15 glycerides (GLs), 8 sphingolipids (SPs), 7 fatty acyls (FAs), 5 sterol lipids (STs), and 1 prenol lipid (PR). Simultaneously, AB23A elevated the levels of 51 out of 1131 abnormally downregulated lipids, including 25 GPs, 4 GLs, 18 SPs, 3 FAs, and 1 ST, indicating the close relationship between these lipids and the efficacy of AB23A (Supplemental files). The results indicated (Fig. 3F) that AB23A played an important role in preventing acute liver injury caused by CCl$_4$ by affecting glycerophospholipid metabolism, sphingolipid metabolism and glycerolipid metabolism in the liver.

Sphingolipids plays a significant role in the transmission of inflammatory signals. Twenty-two sphingolipid levels were improved under the regulation of AB23A (Fig. 4A). Additionally, immunohistochemical analysis revealed an increased abundance of macrophages and enhanced inflammatory response following exposure to CCl$_4$. However, AB23A could alleviate the inflammatory response and reduce macrophage level in the liver (Fig. 4B&C).

3.4. AB23A improved the metabolic function of the liver

TIC of representative samples from various groups in metabolomics

were shown in Fig. 5A. PCA analysis (Fig. 5B) displayed a clear separation of samples among C, M and H groups. Besides, the OPLS-DA score (Fig. 5C) indicated that the C vs. M ($R^2X = 0.682$, $R^2Y = 0.995$, $Q^2 = 0.946$) and M vs. H ($R^2X = 0.560$, $R^2Y = 0.988$, $Q^2 = 0.889$) groups were scattered in distinct areas. It showed that CCl$_4$-induced liver metabolic dysfunction could be modulated by AB23A. 496 up regulated and 271 down regulated metabolites affected by CCl$_4$ were screened and identified using volcano plots (Fig. 5D) and Venn plots (Fig. 5E), while AB23A could regulate 94 (including 30 lipids and lipid-like molecules, 26 organic acids and derivatives, 19 sugars, 10 peptides, 8 nucleosides, nucleotides and analogues, and 1 vitamin) and 42 (including 15 organic acids and derivatives, 5 lipids and lipid-like molecules, 10 peptides, 4 sugars, 7 nucleosides, nucleotides and analogues, and 1 organo-heterocyclic compound) of them to normal levels, respectively (Supplemental files). Pathway enrichment analysis (Fig. 5F) further demonstrated that AB23A primarily exerted its effect against CCl$_4$-induced acute liver injury through the regulation of purine metabolism in the liver.

Purine metabolism is an important pathway involved in cell proliferation and oxidative balance. We observed upregulation of dGMP, GMP, xanthosine, and IDP levels in the model group, while adenosine and inosine levels were downregulated (Fig. 6A). AB23A treatment led to a restoration of their levels. Besides, in the lipidomic analysis, an increase in the content of oxidized phospholipids, a product of lipid peroxidation, was observed in the model group (Fig. 6B). As shown in Fig. 6C, there were a large amount of oxidized phospholipid around the central vein in the model group, whereas the AB23A administration groups exhibited a dose-dependent reduction in their production. Furthermore, the contents of GSH and GPX4 in the liver were significantly reduced ($P < 0.05$), while the level of MDA was significantly increased ($P < 0.01$) (Fig. 6D). AB23A administration significantly reversed the levels of GSH and GPX4 and reduced the content of MDA in the liver ($P < 0.01$), indicating that AB23A had the ability to alleviate liver oxidative stress and protect hepatocytes by reducing lipid peroxidation, thereby reducing the liver toxicity induced by CCl$_4$.

To clarify the changes of differential lipids and metabolites mediated by AB23A in pathways, the normalized peak areas of key metabolites

Fig. 4. AB23A mitigated the inflammatory response induced by CCl$_4$ in the liver. **(A)** The heat map analysis revealed the regulation of AB23A on sphingolipids. **(B)** Representative immunohistochemical staining (macrophage) of liver sections. **(C)** Positive area analysis of immunohistochemical staining (macrophage). *$P < 0.05$, **$P < 0.01$, and ***$P < 0.001$ compared with the model group.
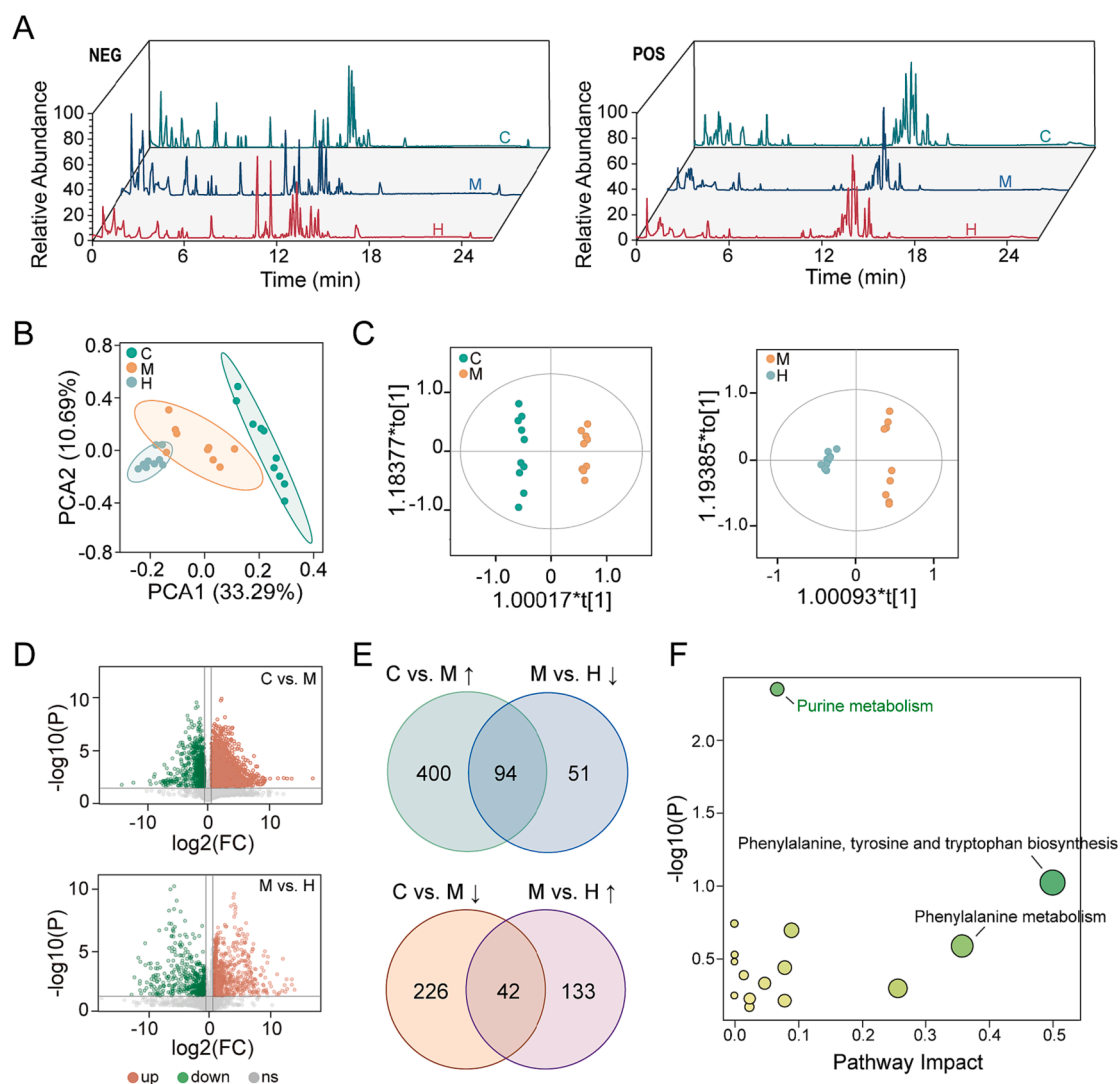
Fig. 5. AB23A could ameliorate liver metabolic disorder caused by CCl$_4$. **(A)** Total ion chromatograms of representative samples from various groups in metabolomics in negative and positive ion modes. **(B)** The PCA score plot showed the metabolism profiling of C, M and H groups were altered. **(C)** The OPLS-DA score plots exhibited distinct separation between the two groups (C vs. M, M vs. H). **(D)** The volcano plot analysis displayed significantly regulated variables between the two groups ($P < 0.05$, fold change > 1.5). **(E)** The Venn plots demonstrated AB23A could regulate the abnormal metabolites caused by CCl$_4$. **(F)** Pathway analysis elucidated the metabolic pathways modulated by AB23A in the liver.

and lipids were quantified (Supplementary materials) and integrated. Using a filtering criterion of a Pearson correlation coefficient greater than 0.8, we constructed a correlation network among key metabolites influenced by AB23A (Fig. 7). The results revealed that the metabolites regulated by AB23A formed a correlated network centered around adenosine and phospholipids, indicating a closely interconnected pattern of changes among these metabolites. Furthermore, the metabolic pathways are illustrated in Fig. 8. Compared with the C group, the M group animals exhibited dysregulated levels of lipids and metabolites in the liver as a result of CCl$_4$ exposure. In lipid metabolism, the levels of LPE, OxPS, OxPC, OxPE, OxPI, PI, TAG, DAG, and SM were significantly increased ($P < 0.05$) in the model group. However, high-dose AB23A administration effectively downregulated these lipids ($P < 0.05$). Conversely, the levels of C1P, LPC, PA, PS, and PE were significantly downregulated ($P < 0.05$) by CCl$_4$, which could be significantly upregulated ($P < 0.05$) in the administration group. Additionally, AB23A demonstrated significant modulation of abnormally upregulated dGMP, GMP, IDP, xanthosine, as well as abnormally downregulated adenosine, inosine, betaine.

4. Discussion

In this study, we investigated the optimal extraction process and the impact of AB23A on CCl$_4$-induced acute liver injury. We found that AB23A could protect the liver by reducing the aggregation of macrophages in the liver, alleviating lipid peroxidation levels in liver cells, and regulating liver metabolism.

AB23A is a protostane-type tetracyclic triterpene. The sample appears as white crystals, insoluble in water, and readily soluble in organic solvents such as methanol and dichloromethane. Studies indicated that excessively harsh conditions can lead to the formation of other triterpenoid components, such as AB23A undergoing side chain cleavage to form alisol A 23-acetate (Zheng et al., 2015). Therefore, we optimized the extraction process of AB23A using both single-factor and response surface methodologies.

The advantages of RSM lie in its ability to use a reduced number of experimental combinations. By establishing mathematical models for continuous analysis of various levels, it enables the identification of optimal solutions for practical applications. As a result, RSM has become an important approach for optimizing traditional Chinese medicine
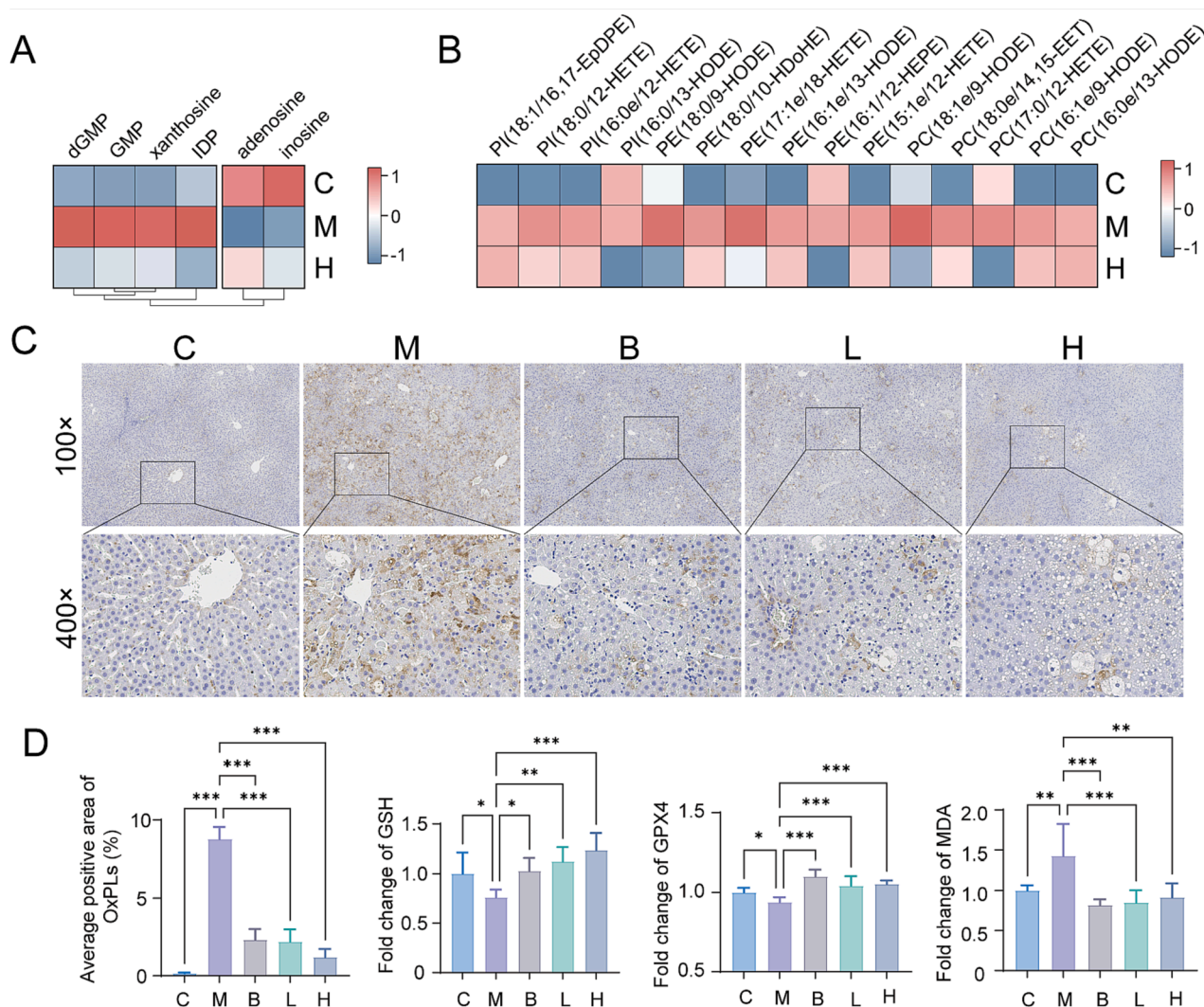
Fig. 6. AB23A could reduce lipid peroxidation caused by CCl4. **(A)** Heat map analysis of key metabolites involved in purine metabolism. **(B)** The heatmap demonstrated the oxidized phospholipid were up-regulated in M group and down-regulated in H group. **(C)** Representative immunohistochemical staining (oxidized phospholipid) of liver sections. **(D)** Positive area analysis of immunohistochemical staining (oxidized phospholipid) and GSH, GPX4, MDA levels in liver. *$P < 0.05$, **$P < 0.01$, and ***$P < 0.001$ compared with the model group.

extraction processes (F. Li et al., 2023; Tasfiyati et al., 2022; Tian et al., 2022). Considering cost investment and industrial implementation, this study investigated the extraction process of reflux extraction. Study had shown that prolonged exposure to high temperatures was detrimental to the stability of AB23A. At a temperature of 70 °C, a small amount of AB23A undergone oxygen ring-opening to convert into alisol A 24-acetate or lost its acetyl group to become alisol B(Zheng et al., 2006). By optimizing the extraction conditions, we found that the optimal conditions included a solid–liquid ratio of 1:13, a reflux extraction of 70 % ethanol, an extraction time of 2 h, and an extraction cycle of 3 cycles.

CCl4 is a typical hepatotoxic substance that is widely used in industrial production, such as insecticide, detergent, extractant, fire extinguishing agent and analytical reagent (Cohen et al., 2023). When the high concentration of CCl4 vapor or solution is introduced into the body, this toxic compound becomes enriched and metabolized within the liver. We investigated the effect of AB23A on carbon tetrachloride induced acute liver injury in rat. After administering high doses of carbon tetrachloride, fat began to accumulate within one hour, afterwards liver necrosis occurred as early as 6 to 12 h (Brautbar and Williams, 2002), and lipid droplets and necrotic liver cells were observed in the model group in our experiment. In addition, toxic metabolites like the trichloromethyl radical (CCl3) and the trichloromethylperoxy radical

(CCl3O2) were produced followed by the CCl4 metabolized under the action of cytochrome P450 in the liver (Brattin et al., 1985; Weber et al., 2003). Simultaneously, the antioxidant enzymes in the liver were insufficient to scavenge free radicals, and the levels of GSH and GPX4 were reduced (Burk et al., 1984; Y. Wang et al., 2023). Consequently, the accumulated free radicals attacked phospholipid molecules within the liver membrane system, resulting in lipid peroxidation and the production of MDA (Ablat et al., 2023; Recknagel et al., 1989). This process caused an increase in cell membrane permeability, ballooning degeneration, and subsequent release of liver enzymes into the blood, leading to elevated levels of AST, ALT, and ALP (Cohen et al., 2023; Paliwal et al., 2023). In our study, AB23A significantly reduced the levels of AST, ALT, and ALP in rat serum, alleviated liver enlargement caused by CCl4, and decreased hepatocellular degeneration, necrosis, and lipid peroxidation. This indicated that AB23A could mitigate acute liver injury induced by CCl4, exerting a hepatoprotective effect. Importantly, compared to the clinically common liver detoxification agent bifendatatum, AB23A achieved a similar therapeutic effect with only one-sixth of the dosage, highlighting its substantial clinical application value.

On the other hand, CCl4 exposure led to lipid deposition and lipid peroxidation in the liver (Smuckler, 1976), suggesting that the liver lipid metabolism disordered. We conducted a lipidomic analysis for liver lipid
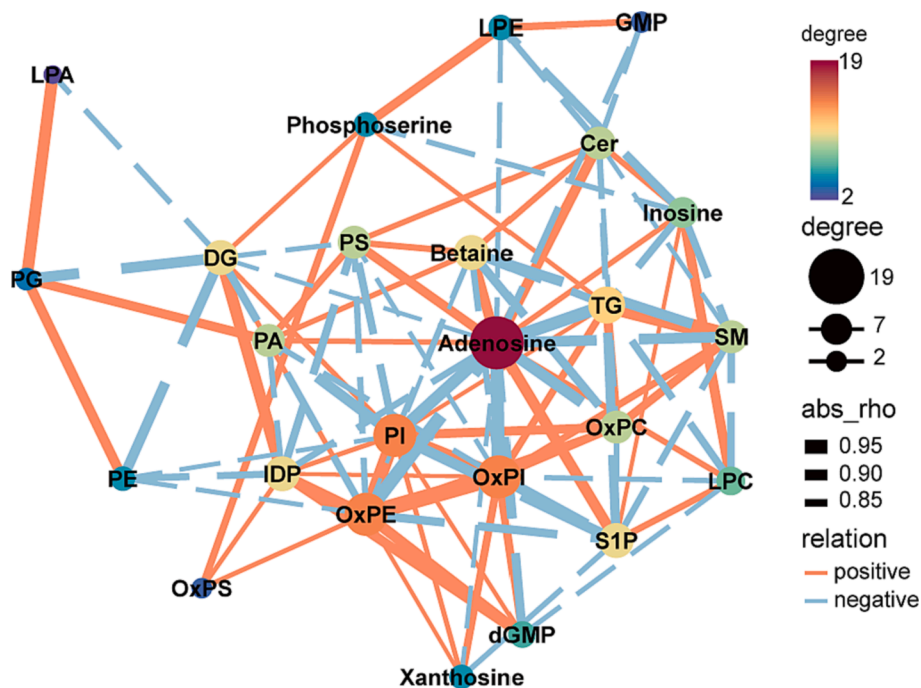
Fig. 7. Correlation network diagram among key metabolites. The size of the circles represents the number of nodes, the thickness of the lines indicates the strength of the correlation. Orange solid lines represent positive correlations between metabolites, while blue dashed lines represent negative correlations.
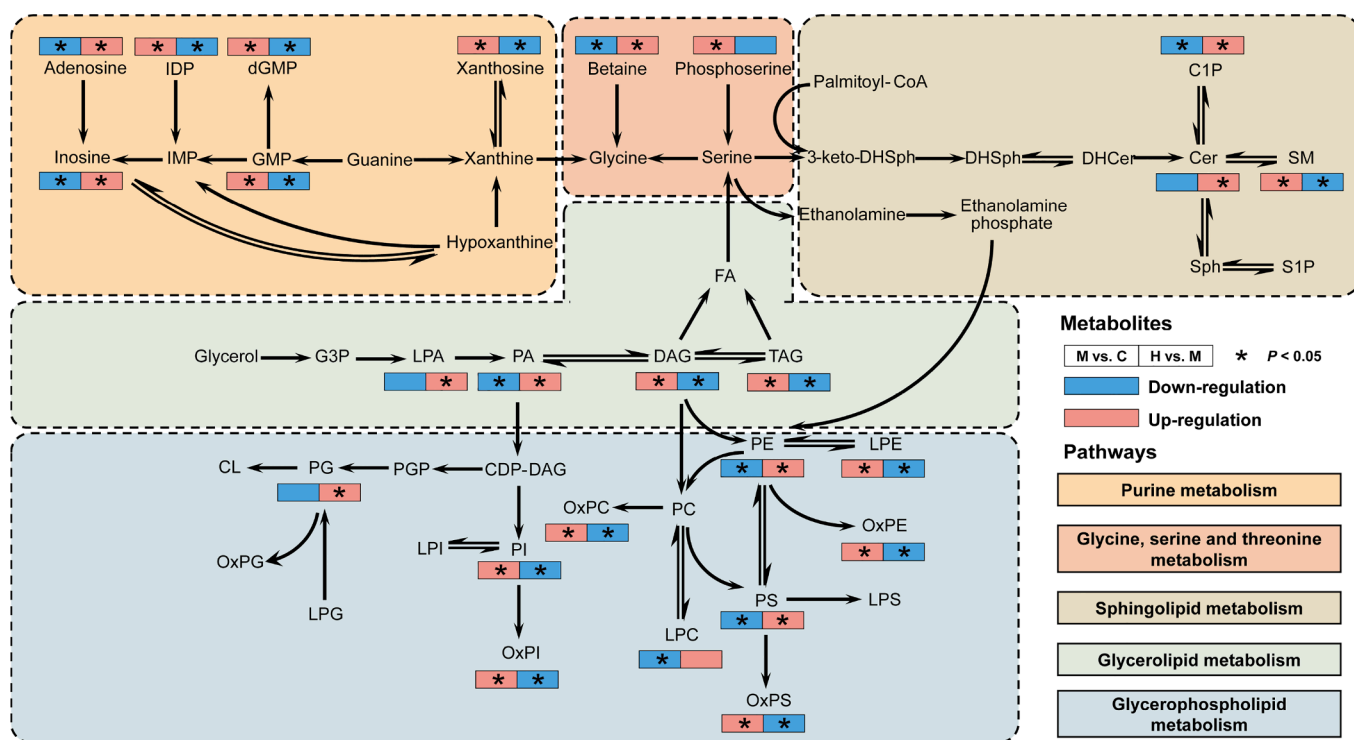

Fig. 8. Schematic representation of the metabolic regulation network illustrating the amelioration of CCl_4-induced acute liver injury by AB23A. The left squares represent the changes in the levels of metabolites affected by CCl_4, while the right squares represent the regulation of these metabolites by AB23A. Red indicates upregulation, and blue indicates downregulation. Asterisks highlight significant changes in metabolite levels ($P < 0.05$). Different background colors represent various metabolic pathways regulated by AB23A.

profiling to clarify the modulation of AB23A on liver lipids. Among the various pathways involved in lipid metabolism, sphingolipid metabolism pathway plays a key role in the process of inflammatory signaling (Maceyka and Spiegel, 2014). Ceramide (Cer), generated in the endoplasmic reticulum, is the center of sphingolipid metabolism and an

essential skeleton of complex sphingolipids (Gaggini et al., 2022; Hannun and Obeid, 2011). In our study, AB23A treatment upregulated the level of Cer, which can accumulate in in invagination of the cell membrane to facilitate signaling and enhance the stability of the cell membrane structure (Józefowski et al., 2010; Rozenova et al., 2010). But

excessive Cer accumulation may lead to cell apoptosis or autophagy (Mir and Thirunavukkarasu, 2023; Obeid et al., 1993). Ceramide can be converted to sphingomyelin (SM) through the action of sphingomyelin synthase (SMS). Intriguingly, AB23A treatment resulted in a reduction in SM levels, which may be attributed to the downregulation of SMS activity. Studies have shown that overexpressed SMS increased inflammatory biomarkers in atherosclerotic plaques and aggravated the instability of arterial plaques (Zhao et al., 2012). In this regard, ceramide accumulation has an anti-inflammatory effect, while SMS plays a significant role in the inflammatory signal transmission. Unlike ceramide, most ceramide-1-phosphate (C1P) is synthesized in the golgiosome and transported to the plasma membrane by C1P transfer proteins. C1P has been shown to inhibit cell apoptosis (Gómez-Muñoz, 2006), stimulate cellular DNA synthesis (Gomez-Muñoz et al., 1997), and promote cell proliferation. The increased content of C1P observed in the administration group may be associated with enhanced damage repair in hepatocytes.

In this study, abundant lipids were enriched in glycerolipid metabolism and glycerophospholipid metabolism. The increase of lysophosphatidic acid (LPA) is of great significance for liver protection, as it increases liver GSH and alleviates JNK, ERK, and SK3 β phosphorylation, resulting in improved antioxidant capacity and reduced release of proinflammatory factors (Bae et al., 2017). LPA may also be involved in the proliferation of hepatocytes and recovery of cellular function (Simo et al., 2014). Furthermore, LPA can be converted to phosphatidic acid (PA) in the presence of glycerol-3-phosphate acyltransferase (GPAT), and PA have the potential to promote cell proliferation by regulating glycogen synthase kinase 3 beta (GSK3 β) to alleviate liver injury (Clemens et al., 2019; Lutkewitte et al., 2018). Protein kinase C (PKC), which can be activated by diacylglycerol (DAG) and phosphatidylserine (PS) (Rosse et al., 2010), is crucial in the regulation of cell proliferation, differentiation, and apoptosis, as well as in inflammatory and cellular damage (Alchera et al., 2010; Tonetti et al., 1994). Due to the toxicity of CCl$_4$ to the liver, levels of DAG and PS were increased, leading to the activation of PKC and triggering the NF-κB pathway (Asehnoune et al., 2005; Toriumi et al., 2013), which induces inflammatory responses. However, AB23A administration effectively regulated DAG and PS levels back to normal, reducing PKC-induced inflammatory responses and cellular damage. Triacylglycerol (TG) was accumulated in the liver due to the damage of hepatocytes, while the TG level in the administration group was reduced, suggesting that AB23A had a protective effect against CCl$_4$ induced acute liver injury. In addition to glycerolipid metabolism, we also observed alterations in glycerophospholipid metabolism in the model group, where severe lipid peroxidation occurred due to the conversion of CCl$_4$ to toxic free radicals like trichloromethyl radical (CCl$_3$) and trichloromethyl peroxide radical (CCl$_3$O$_2$) by cytochrome P450 enzymes. This led to the oxidation of phospholipids (PLs), which are vital components of the biomembrane system, into oxidized phospholipids (OxPLs) (Slater et al., 1985; Unsal et al., 2021). AB23A increased the phospholipid content and significantly reduced the level of oxidized phospholipid, thereby protecting the membrane structure and maintaining normal physiological activities of hepatocytes. These effects might be related to the upregulation of antioxidant metabolites, such as betaine and adenosine, or other related proteins.

As a vital metabolic organ, the liver plays an important role not only in lipid metabolism but also in protein metabolism, glucose metabolism and vitamin metabolism. We further analyzed the metabolic dysfunction caused by CCl$_4$ through metabolomics to reveal the protective effect of AB23A on acute liver injury. In the glycine, serine and threonine metabolism, although serine was not screened as a regulated differential metabolite in this experiment, the content of its upstream metabolite, phosphoserine, was down regulated. This indicated an increase in the activity of phosphoprotein phosphatase (PPP), an important regulator of cell mitosis (Nilsson, 2019), suggesting enhanced liver recovery. After AB23A administration, the level of betaine was increased. Betaine, a

trimethyl derivative of glycine, serves as an important methyl donor in one-carbon metabolism within the liver. In hepatocyte mitochondria, betaine participates in the synthesis of methionine and glycine through the methionine cycle, facilitating protein synthesis and glutathione production (Martínez et al., 2017), thereby enhancing the liver's antioxidant capacity. Furthermore, betaine has been shown to inhibit the NF-κB signaling pathway and activate the NLRP3 inflammasome, exerting anti-inflammatory effects (Go et al., 2007; Kathirvel et al., 2010).

Purine is an essential component of DNA and RNA, as well as providing cells with necessary energy and cofactors to promote cell survival and proliferation (Wang et al., 2020; Di Virgilio and Adinolfi, 2017). The Purine metabolism pathway also serves as a crucial cellular communication pathway mediated by extracellular nucleotides and nucleosides (Coutinho-Silva and Savio, 2021; Idzko et al., 2014). Under physiological or pathological conditions, triphosphate and diphosphate nucleotides are released, leading to the activation of type 2 purine receptor (P2 receptor), which, in turn, trigger the production of reactive oxygen species (ROS) and reactive nitrogen species (Shen et al., 2000), disrupting the cell's redox balance. With the activation of P2 receptor, adenosine triphosphate (ATP) and adenosine diphosphate (ADP) are hydrolyzed to adenosine monophosphate (AMP) by ectonucleoside triphosphate diphosphohydrolase 1/CD39, and then to adenosine by ecto-5′-nucleotidase/CD73. Upregulation of these two enzymes can alleviate ATP-induced oxidative stress and ROS-induced cell damage (al-Rashida and Iqbal, 2014; Robson et al., 2006). In addition, the increased adenosine levels activate adenosine receptors (Ramkumar et al., 2001), maintaining redox homeostasis by reducing ROS production and increasing antioxidant enzymes. Studies have also revealed that inosine, the hydrolysate of ATP, exerts anti-inflammatory effects through adenosine receptor activation (Gomez and Sitkovsky, 2003; Kim and Jo, 2022; Samami et al., 2023). On the other hand, with the production of ROS, xanthine oxidase converted hypoxanthine to xanthine, and eventually to uric acid, which also have a certain resistance to oxidative stress (Xing et al., 2023; Furuhashi, 2020; Glantzounis et al., 2005).

According to the metabolic network diagram, the protective effect of AB23A on CCl$_4$-induced acute liver injury was the result of interaction and co-regulation of glycine, serine and threonine metabolism, sphingolipid metabolism, glycerolipid metabolism, and glycerophospholipid metabolism. Purine metabolism is an important pathway involved in cell proliferation and oxidative balance. Glycine, serine and threonine metabolism, as the central metabolic pathway, is an essential component in the maintenance of cell normal physiological activity. Sphingolipid metabolism pathway plays a key role in the process of inflammatory signaling. Glycerolipids and glycerophospholipids are not only vital components of cell structure, but also take an important part in the cell growth cycle. Overall, the toxicity reduction mediated by AB23A may be attributed to its ability to decrease inflammation, increase antioxidant levels, and enhance the recovery ability of hepatocytes.

Prior investigations indicated that AB23A could alleviate CCl$_4$-induced liver damage by activating FXR receptors to regulate bile acid metabolism (Meng et al., 2015). Additionally, studies reported that acute liver injury induced by CCl$_4$ was often associated with ferroptosis (Bi et al., 2023; Fan et al., 2023; Y. Li et al., 2023; Wei et al., 2022). Interestingly, in our study, with the increasing dosage of AB23A, liver MDA levels significantly decreased, and GSH and GPX4 levels significantly increased. Immunohistochemical analysis and lipidomics results also showed a significant downregulation of liver oxidative phospholipid levels. This suggested that the protective effect of AB23A against CCl$_4$-induced acute liver injury might also be related to the inhibition of ferroptosis, but further verification is still needed.

5. Conclusion

The extraction process and protective activity against acute liver

injury of AB23A were investigated for its exploitation. The optimization of the extraction protocol conducted using the RSM allowed us to evaluate the maximum extractable AB23A amount contained in Alismatis Rhizoma. (2.90 mg/g). Furthermore, our study highlighted the protective effects of AB23A against CCl_4-induced acute liver injury in rats. By regulating glycerophospholipid metabolism, AB23A effectively reduced the inflammatory response, while modulation of purine metabolism enhanced antioxidant capacity, leading to the attenuation of lipid peroxidation. Nevertheless, further investigations are necessary to uncover the precise molecular mechanisms involved. These findings established a foundation for the therapeutic application of AB23A in the clinical treatment of acute liver injury.

Author contributions

Participated in research design: Miaomiao Jiang, Peng Lei. Conducted experiment: Peng Lei, Zhirong Zhou, Jierong Pei, Li Jia. Performed data analysis: Peng Lei. Editing and writing of the manuscript, designing and drawing of tables and figures: Peng Lei, Miaomiao Jiang. All data were generated in-house, and no paper mill was used. All authors agree to be accountable for all aspects of work ensuring integrity and accuracy.

CRediT authorship contribution statement

Peng Lei: Formal analysis, Methodology, Visualization, Writing – original draft. **Zhirong Zhou:** Methodology, Data curation, Project administration. **Jierong Pei:** Resources, Software. **Li Jia:** Investigation, Supervision. **Lifeng Han:** Validation. **Miaomiao Jiang:** Conceptualization, Funding acquisition. Writing – review & editing.

Declaration of competing interest

The authors declare that they have no known competing financial interests or personal relationships that could have appeared to influence the work reported in this paper.

Acknowledgement

Appendix A. Supplementary data

Supplementary data to this article can be found online at https://doi.org/10.1016/j.arabjc.2023.105479.

References

Ablat, N., Ablimit, M., Abudoukadier, A., Kadeer, B., Maihemuti, A., Bakewaiyi, A., Tuerxun, A., Aihemaiti, A., 2023. Liver protection and hemostatic effects of medicinal plant Arnebia euchroma (Royle) I.M.Johnst extract in a rat model. J. Ethnopharmacol. 300, 115739 https://doi.org/10.1016/j.jep.2022.115739.

Alchera, E., Dal Ponte, C., Imarisio, C., Albano, E., Carini, R., 2010. Molecular mechanisms of liver preconditioning. World J. Gastroenterol. 16, 6058–6067. https://doi.org/10.3748/wjg.v16.i48.6058.

al-Rashida, M., Iqbal, J., 2014. Therapeutic potentials of ecto-nucleoside triphosphate diphosphohydrolase, ecto-nucleotide pyrophosphatase/phosphodiesterase, ecto-5'-nucleotidase, and alkaline phosphatase inhibitors. Med Res Rev 34, 703–743. https://doi.org/10.1002/med.21302.

Aoyagi, R., Ikeda, K., Isobe, Y., Arita, M., 2017. Comprehensive analyses of oxidized phospholipids using a measured MS/MS spectra library. J. Lipid Res. 58, 2229–2237. https://doi.org/10.1194/jlr.D077123.

Asehnoune, K., Strassheim, D., Mitra, S., Yeol Kim, J., Abraham, E., 2005. Involvement of PKCalpha/beta in TLR4 and TLR2 dependent activation of NF-kappaB. Cell. Signal. 17, 385–394. https://doi.org/10.1016/j.cellsig.2004.08.005.

Bae, G.H., Lee, S.K., Kim, H.S., Lee, M., Lee, H.Y., Bae, Y.-S., 2017. Lysophosphatidic acid protects against acetaminophen-induced acute liver injury. Exp. Mol. Med. 49, e407.

Bai, J., Xie, N., Hou, Y., Chen, X., Hu, Y., Zhang, Y., Meng, X., Wang, X., Tang, C., 2022. The enhanced mitochondrial dysfunction by cantleyoside confines inflammatory

response and promotes apoptosis of human HFLS-RA cell line via AMPK/Sirt 1/NF-κB pathway activation. Biomed. Pharmacother. 149, 112847 https://doi.org/10.1016/j.biopha.2022.112847.

Bi, Y., Liu, S., Qin, X., Abudureyimu, M., Wang, L., Zou, R., Ajoolabady, A., Zhang, W., Peng, H., Ren, J., Zhang, Y., 2023. FUNDC1 interacts with GPx4 to govern hepatic ferroptosis and fibrotic injury through a mitophagy-dependent manner, 00063–2 J. Adv. Res. S2090–1232 (23). https://doi.org/10.1016/j.jare.2023.02.012.

Brattin, W.J., Glende, E.A., Recknagel, R.O., 1985. Pathological mechanisms in carbon tetrachloride hepatotoxicity. J. Free Radic. Biol. Med. 1, 27–38. https://doi.org/10.1016/0748-5514(85)90026-1.

Brautbar, N., Williams, J., 2002. Industrial solvents and liver toxicity: Risk assessment, risk factors and mechanisms. Int. J. Hyg. Environ. Health 205, 479–491. https://doi.org/10.1078/1438-4639-00175.

Burk, R.F., Lane, J.M., Patel, K., 1984. Relationship of oxygen and glutathione in protection against carbon tetrachloride-induced hepatic microsomal lipid peroxidation and covalent binding in the rat. Rationale for the use of hyperbaric oxygen to treat carbon tetrachloride ingestion. J. Clin. Invest. 74, 1996–2001. https://doi.org/10.1172/JCI111621.

Chen, Y., Lu, J., Xie, Z., Tang, J., Lian, X., Li, X., 2022. The Mechanism of Alisol B23 Acetate Inhibiting Lung Cancer: Targeted Regulation of CD11b/CD18 to Influence Macrophage Polarization. Drug Des. Devel. Ther. 16, 3677–3689. https://doi.org/10.2147/DDDT.S375073.

Clemens, M.M., Kennon-McGill, S., Apte, U., James, L.P., Finck, B.N., McGill, M.R., 2019. The inhibitor of glycerol 3-phosphate acyltransferase FSG67 blunts liver regeneration after acetaminophen overdose by altering GSK3β and Wnt/β-catenin signaling. Food Chem. Toxicol. 125, 279–288. https://doi.org/10.1016/j.fct.2019.01.014.

Cohen, S.M., Bevan, C., Gollapudi, B., Klaunig, J.E., 2023. Evaluation of the carcinogenicity of carbon tetrachloride. Journal of Toxicology and Environmental Health, Part B 1–29. https://doi.org/10.1080/10937404.2023.2220147.

Coutinho-Silva, R., Savio, L.E.B., 2021. Purinergic signalling in host innate immune defence against intracellular pathogens. Biochem. Pharmacol. 187, 114405 https://doi.org/10.1016/j.bcp.2021.114405.

Di Virgilio, F., Adinolfi, E., 2017. Extracellular purines, purinergic receptors and tumor growth. Oncogene 36, 293–303. https://doi.org/10.1038/onc.2016.206.

Fan, X., Wang, X., Hui, Y., Zhao, T., Mao, L., Cui, B., Zhong, W., Sun, C., 2023. Genipin protects against acute liver injury by abrogating ferroptosis via modification of GPX4 and ALOX15-launched lipid peroxidation in mice. Apoptosis 28, 1469–1483. https://doi.org/10.1007/s10495-023-01867-9.

Fernández, J., Silván, B., Entrialgo-Cadierno, R., Villar, C.J., Capasso, R., Uranga, J.A., Lombó, F., Abalo, R., 2021. Antiproliferative and palliative activity of flavonoids in colorectal cancer. Biomed. Pharmacother. 143, 112241 https://doi.org/10.1016/j.biopha.2021.112241.

Ferrarini, E.G., Paes, R.S., Baldasso, G.M., de Assis, P.M., Gouvêa, M.C., Cicco, P.D., Raposo, N.R.B., Capasso, R., Moreira, E.L.G., Dutra, R.C., 2022. Broad-spectrum cannabis oil ameliorates reserpine-induced fibromyalgia model in mice. Biomed. Pharmacother. 154, 113552 https://doi.org/10.1016/j.biopha.2022.113552.

Foroutan, T., Ahmadi, F., Moayer, F., Khalvati, S., 2020. Effects of intraperitoneal injection of magnetic graphene oxide on the improvement of acute liver injury induced by CCl_4. Biomater Res 24, 14. https://doi.org/10.1186/s40824-020-00192-5.

Fu, Y., Feng, H., Ding, X., Meng, Q.-H., Zhang, S.-R., Li, J., Chao, Y., Ji, T.-T., Bi, Y.-H., Zhang, W.-W., Chen, Q., Zhang, Y.-H., Feng, Y.-L., Bian, H.-M., 2022. Alisol B 23-acetate adjusts bile acid metabolism via hepatic FXR-BSEP signaling activation to alleviate atherosclerosis. Phytomedicine 101, 154120. https://doi.org/10.1016/j.phymed.2022.154120.

Furuhashi, M., 2020. New insights into purine metabolism in metabolic diseases: role of xanthine oxidoreductase activity. E827–E834 Am. J. Phys. Endocrinol. Metab. 319. https://doi.org/10.1152/ajpendo.00378.2020.

Gaggini, M., Ndreu, R., Michelucci, E., Rocchiccioli, S., Vassalle, C., 2022. Ceramides as Mediators of Oxidative Stress and Inflammation in Cardiometabolic Disease. Int. J. Mol. Sci. 23, 2719. https://doi.org/10.3390/ijms23052719.

Glantzounis, G.K., Tsimoyiannis, E.C., Kappas, A.M., Galaris, D.A., 2005. Uric acid and oxidative stress. Curr. Pharm. Des. 11, 4145–4151. https://doi.org/10.2174/1381612057749132555.

Go, E.K., Jung, K.J., Kim, J.M., Lim, H., Lim, H.K., Yu, B.P., Chung, H.Y., 2007. Betaine modulates age-related NF-kappaB by thiol-enhancing action. Biol. Pharm. Bull. 30, 2244–2249. https://doi.org/10.1248/bpb.30.2244.

Gomez, G., Sitkovsky, M.V., 2003. Differential requirement for A2a and A3 adenosine receptors for the protective effect of inosine in vivo. Blood 102, 4472–4478. https://doi.org/10.1182/blood-2002-11-3624.

Gómez-Muñoz, A., 2006. Ceramide 1-phosphate/ceramide, a switch between life and death. BBA 1758, 2049–2056. https://doi.org/10.1016/j.bbamem.2006.05.011.

Gomez-Muñoz, A., Frago, L.M., Alvarez, L., Varela-Nieto, I., 1997. Stimulation of DNA synthesis by natural ceramide 1-phosphate. Biochem. J 325 (Pt 2), 435–440. https://doi.org/10.1042/bj3250435.

Hannun, Y.A., Obeid, L.M., 2011. Many ceramides. J. Biol. Chem. 286, 27855–27862. https://doi.org/10.1074/jbc.R111.254359.

He, Z., Li, X., Wang, Z., Cao, Y., Han, S., Li, N., Cai, J., Cheng, S., Liu, Q., 2023. Protective effects of luteolin against amyloid beta-induced oxidative stress and mitochondrial impairments through peroxisome proliferator-activated receptor γ-dependent mechanism in Alzheimer's disease. Redox Biol. 66, 102848 https://doi.org/10.1016/j.redox.2023.102848.

Heimberg, M., Weinstein, I., 1962. A mechanism for the induction by carbon tetrachloride of fatty liver in the rat. Biochem. Pharmacol. 11, 163–165. https://doi.org/10.1016/0006-2952(62)90104-1.

Idzko, M., Ferrari, D., Eltzschig, H.K., 2014. Nucleotide signalling during inflammation. Nature 509, 310–317. https://doi.org/10.1038/nature13085.

Jia, L., Zhang, M., Wang, P., Wang, L., Lei, P., Du, R., Han, L., Zhang, P., Wang, Y., Jiang, M., 2022. Alismatis Rhizoma methanolic extract—Effects on metabolic syndrome and mechanisms of triterpenoids using a metabolomic and lipidomic approach. Front. Pharmacol. 13, 983428 https://doi.org/10.3389/fphar.2022.983428.

Józefowski, S., Czerkies, M., Łukasik, A., Bielawska, A., Bielawski, J., Kwiatkowska, K., Sobota, A., 2010. Ceramide and ceramide 1-phosphate are negative regulators of TNF-α production induced by lipopolysaccharide. J. Immunol. 185, 6960–6973. https://doi.org/10.4049/jimmunol.0902926.

Kathirvel, E., Morgan, K., Nandgiri, G., Sandoval, B.C., Caudill, M.A., Bottiglieri, T., French, S.W., Morgan, T.R., 2010. Betaine improves nonalcoholic fatty liver and associated hepatic insulin resistance: a potential mechanism for hepatoprotection by betaine. G1068-1077 Am. J. Physiol. Gastrointest. Liver Physiol. 299. https://doi.org/10.1152/ajpgi.00249.2010.

Kim, I.S., Jo, E.-K., 2022. Inosine: A bioactive metabolite with multimodal actions in human diseases. Front. Pharmacol. 13, 1043970. https://doi.org/10.3389/fphar.2022.1043970.

Lei, P., Mwangi, C.N., Cao, Y., Chen, J., Huang, Y., Wang, Y., Zhu, Y., Fan, G., Jiang, M., 2023. Investigating the mechanism of action of Danhong injection and its components against myocardial ischemia-reperfusion injury. Acupuncture and Herbal Medicine 10.1097/HM9.0000000000000040. https://doi.org/10.1097/HM9.0000000000000040.

Lei, P., Lü, J., Yao, T., Zhang, P., Chai, X., Wang, Y., Jiang, M., 2023a. Verbascoside exerts an anti-atherosclerotic effect by regulating liver glycerophospholipid metabolism. Food Sci. Human Wellness 12, 2314–2323. https://doi.org/10.1016/j.fshw.2023.03.035.

Li, F., Xiao, L., Lin, X., Dai, J., Hou, J., Wang, L., 2023a. Deep Eutectic Solvents-Based Ultrasound-Assisted Extraction of Antioxidants from Kudingcha (llex kudingcha C.J. Tseng): Process Optimization and Comparison with Other Methods. Foods 12, 1872. https://doi.org/10.3390/foods12091872.

Li, Y., Yu, P., Fu, W., Wang, S., Zhao, W., Ma, Y., Wu, Y., Cui, H., Yu, X., Fu, L., Xu, H., Sui, D., 2023b. Ginsenoside Rd Inhibited Ferroptosis to Alleviate CCl$_4$-Induced Acute Liver Injury in Mice via cGAS/STING Pathway. Am. J. Chin. Med. 51, 91–105. https://doi.org/10.1142/S0192415X23500064.

Lutkewitte, A.J., Schweitzer, G.G., Kennon-McGill, S., Clemens, M.M., James, L.P., Jaeschke, H., Finck, B.N., McGill, M.R., 2018. Lipin deactivation after acetaminophen overdose causes phosphatidic acid accumulation in liver and plasma in mice and humans and enhances liver regeneration. Food Chem. Toxicol. 115, 273–283. https://doi.org/10.1016/j.fct.2018.03.014.

Maceyka, M., Spiegel, S., 2014. Sphingolipid metabolites in inflammatory disease. Nature 510, 58–67. https://doi.org/10.1038/nature13475.

Martínez, Y., Li, X., Liu, G., Bin, P., Yan, W., Más, D., Valdivié, M., Hu, C.-A.-A., Ren, W., Yin, Y., 2017. The role of methionine on metabolism, oxidative stress, and diseases. Amino Acids 49, 2091–2098. https://doi.org/10.1007/s00726-017-2494-2.

Meng, Q., Chen, X., Wang, C., Liu, Q., Sun, H., Sun, P., Huo, X., Liu, Z., Liu, K., 2015. Protective effects of alisol B 23-acetate from edible botanical Rhizoma alismatis against carbon tetrachloride-induced hepatotoxicity in mice. Food Funct. 6, 1241–1250. https://doi.org/10.1039/C5FO00082C.

Meng, N., Lyu, Y., Zhang, X., Chai, X., Li, K., Wang, Y., 2022. The exciting and magical journey of components from compound formulae to where they fight. Acupuncture and Herbal Medicine 2, 240. https://doi.org/10.1097/HM9.0000000000000047.

Mir, I.H., Thirunavukkarasu, C., 2023. The relevance of acid sphingomyelinase as a potential target for therapeutic intervention in hepatic disorders: current scenario and anticipated trends. Arch. Toxicol. 1–19 https://doi.org/10.1007/s00204-023-03529-w.

Nilsson, J., 2019. Protein phosphatases in the regulation of mitosis. J. Cell Biol. 218, 395–409. https://doi.org/10.1083/jcb.201809138.

Obeid, L.M., Linardic, C.M., Karolak, L.A., Hannun, Y.A., 1993. Programmed cell death induced by ceramide. Science 259, 1769–1771. https://doi.org/10.1126/science.8456305.

Paliwal, V.M., Kundu, S., Kulhari, U., Jala, A., Ishteyaque, S., Borkar, R.M., Mugale, M. N., Murty, U.S., Sahu, B.D., 2023. Alternanthera brasiliana L. extract alleviates carbon tetrachloride-induced liver injury and fibrotic changes in mice: Role of matrix metalloproteinases and TGF-β/Smad axis. J. Ethnopharmacol. 303, 115992 https://doi.org/10.1016/j.jep.2022.115992.

Pang, Z., Chong, J., Zhou, G., de Lima Morais, D.A., Chang, L., Barrette, M., Gauthier, C., Jacques, P.-É., Li, S., Xia, J., 2021. MetaboAnalyst 5.0: narrowing the gap between raw spectra and functional insights. W388–W396 Nucleic Acids Res. 49. https://doi.org/10.1093/nar/gkab382.

Qu, J., Qiu, B., Zhang, Y., Hu, Y., Wang, Z., Guan, Z., Qin, Y., Sui, T., Wu, F., Li, B., Han, W., Peng, X., 2023. The tumor-enriched small molecule gambogic amide suppresses glioma by targeting WDR1-dependent cytoskeleton remodeling. Sig Transduct Target Ther 8, 1–15. https://doi.org/10.1038/s41392-023-01666-3.

Ramkumar, V., Hallam, D.M., Nie, Z., 2001. Adenosine, oxidative stress and cytoprotection. Jpn. J. Pharmacol. 86, 265–274. https://doi.org/10.1254/jjp.86.265.

Recknagel, R.O., Glende, E.A., Dolak, J.A., Waller, R.L., 1989. Mechanisms of carbon tetrachloride toxicity. Pharmacol. Ther. 43, 139–154. https://doi.org/10.1016/0163-7258(89)90050-8.

Robson, S.C., Sévigny, J., Zimmermann, H., 2006. The E-NTPDase family of ectonucleotidases: Structure function relationships and pathophysiological significance. Purinergic Signal 2, 409–430. https://doi.org/10.1007/s11302-006-9003-5.

Rosse, C., Linch, M., Kermorgant, S., Cameron, A.J.M., Boeckeler, K., Parker, P.J., 2010. PKC and the control of localized signal dynamics. Nat. Rev. Mol. Cell Biol. 11, 103–112. https://doi.org/10.1038/nrm2847.

Rozenova, K.A., Deevska, G.M., Karakashian, A.A., Nikolova-Karakashian, M.N., 2010. Studies on the role of acid sphingomyelinase and ceramide in the regulation of tumor necrosis factor alpha (TNFalpha)-converting enzyme activity and TNFalpha secretion in macrophages. J. Biol. Chem. 285, 21103–21113. https://doi.org/10.1074/jbc.M109.080671.

Şahin, T.Ö., Yılmaz, B., Yeşilyurt, N., Cicia, D., Szymanowska, A., Amero, P., Ağagündüz, D., Capasso, R., 2023. Recent insights into the nutritional immunomodulation of cancer-related microRNAs. Phytother. Res. 37, 4375–4397. https://doi.org/10.1002/ptr.7937.

Samami, E., Aleebrahim-Dehkordi, E., Mohebalizadeh, M., Yaribash, S., Saghazadeh, A., Rezaei, N., 2023. Inosine, gut microbiota, and cancer immunometabolism. Am. J. Phys. Endocrinol. Metab. 324, E1–E8. https://doi.org/10.1152/ajpendo.00207.2022.

Shao, C., Fu, B., Ji, N., Pan, S., Zhao, X., Zhang, Z., Qiu, Y., Wang, R., Jin, M., Wen, K., Kong, D., 2018. Alisol B 23-Acetate Inhibits IgE/Ag-Mediated Mast Cell Activation and Allergic Reaction. Int. J. Mol. Sci. 19, 4092. https://doi.org/10.3390/ijms19124092.

Shen, J.Z., Zheng, X.F., Kwan, C.Y., 2000. Evidence for P(2)-purinoceptors contribution in H(2)O(2)-induced contraction of rat aorta in the absence of endothelium. Cardiovasc. Res. 47, 574–585. https://doi.org/10.1016/S0008-6363(00)00123-1.

Sheng, C., Guo, Y., Ma, J., Hong, E.-K., Zhang, B., Yang, Y., Zhang, X., Zhang, D., 2022. Metabolomic Profiling Reveals Protective Effects and Mechanisms of Sea Buckthorn Sterol against Carbon Tetrachloride-Induced Acute Liver Injury in Rats. Molecules 27, 2224. https://doi.org/10.3390/molecules27072224.

Simo, K.A., Niemeyer, D.J., Hanna, E.M., Swet, J.H., Thompson, K.J., Sindram, D., Iannitti, D.A., Eheim, A.L., Sokolov, E., Zuckerman, V., McKillop, I.H., 2014. Altered lysophosphatidic acid (LPA) receptor expression during hepatic regeneration in a mouse model of partial hepatectomy. HPB (Oxford) 16, 534–542. https://doi.org/10.1111/hpb.12176.

Slater, T.F., Cheeseman, K.H., Ingold, K.U., 1985. Carbon tetrachloride toxicity as a model for studying free-radical mediated liver injury. Philos. Trans. R. Soc. Lond. B Biol. Sci. 311, 633–645. https://doi.org/10.1098/rstb.1985.0169.

Smuckler, E.A., 1976. Structural and functional changes in acute liver injury. Environ. Health Perspect. 15, 13–25.

Tasfiyati, A.N., Antika, L.D., Dewi, R.T., Septama, A.W., Sabarudin, A., Ernawati, T., 2022. An experimental design approach for the optimization of scopoletin extraction from Morinda citrifolia L. using accelerated solvent extraction. Talanta 238, 123010. https://doi.org/10.1016/j.talanta.2021.123010.

Tian, M., Wang, L., Dong, Z., Wang, X., Qin, X., Wang, C., Wang, J., Huang, Q., 2022. Preparation, structural characterization, antioxidant activity and protection against cisplatin-induced acute kidney injury by polysaccharides from the lateral root of Aconitum carmichaelii. Front. Pharmacol. 13, 1002774. https://doi.org/10.3389/fphar.2022.1002774.

Tonetti, D.A., Henning-Chubb, C., Yamanishi, D.T., Huberman, E., 1994. Protein kinase C-beta is required for macrophage differentiation of human HL-60 leukemia cells. J. Biol. Chem. 269, 23230–23235.

Toriumi, K., Horikoshi, Y., Yoshiyuki Osamura, R., Yamamoto, Y., Nakamura, N., Takekoshi, S., 2013. Carbon tetrachloride-induced hepatic injury through formation of oxidized diacylglycerol and activation of the PKC/NF-κB pathway. Lab. Invest. 93, 218–229. https://doi.org/10.1038/labinvest.2012.145.

Tsugawa, H., Ikeda, K., Takahashi, M., Satoh, A., Mori, Y., Uchino, H., Okahashi, N., Yamada, Y., Tada, I., Bonini, P., Higashi, Y., Okazaki, Y., Zhou, Z., Zhu, Z.-J., Koelmel, J., Cajka, T., Fiehn, O., Saito, K., Arita, M., Arita, M., 2020. A lipidome atlas in MS-DIAL 4. Nat. Biotechnol. 38, 1159–1163. https://doi.org/10.1038/s41587-020-0531-2.

Unsal, V., Cicek, M., Sabancilar, İ., 2021. Toxicity of carbon tetrachloride, free radicals and role of antioxidants. Rev. Environ. Health 36, 279–295. https://doi.org/10.1515/reveh-2020-0048.

Wang, Y., Deng, X., Liu, Y., Wang, Y., Luo, X., Zhao, T., Wang, Z., Cheng, G., 2023b. Protective effect of Anneslea fragrans ethanolic extract against CCl$_4$-induced liver injury by inhibiting inflammatory response, oxidative stress and apoptosis. Food Chem. Toxicol. 175, 113752 https://doi.org/10.1016/j.fct.2023.113752.

Wang, P., Jia, J., Zhang, D., 2020. Purinergic signalling in liver diseases: Pathological functions and therapeutic opportunities. JHEP Rep 2, 100165. https://doi.org/10.1016/j.jhepr.2020.100165.

Wang, W., Zhang, Y., Liu, X., Liu, Z., Jia, L., Zhang, J., 2023a. Polysaccharides from Oudemansiella radicata residues attenuate carbon tetrachloride-induced liver injury. Int. J. Biol. Macromol. 242, 124823 https://doi.org/10.1016/j.ijbiomac.2023.124823.

Watts, R.W.E., 1950. Carbon tetrachloride poisoning. Lancet 1, 66. https://doi.org/10.1016/s0140-6736(50)90006-7.

Weber, L.W.D., Boll, M., Stampfl, A., 2003. Hepatotoxicity and Mechanism of Action of Haloalkanes: Carbon Tetrachloride as a Toxicological Model. Crit. Rev. Toxicol. 33, 105–136. https://doi.org/10.1080/713611034.

Wei, Y., Wang, H., Zhang, Y., Gu, J., Zhang, X., Gong, X., Hao, Z., 2022. Comprehensive Effect of Carbon Tetrachloride and Reversal of Gandankang Formula in Mice Liver: Involved in Oxidative Stress, Excessive Inflammation, and Intestinal Microflora. Antioxidants (basel) 11, 2234. https://doi.org/10.3390/antiox11112234.

Wishart, D.S., Guo, A., Oler, E., Wang, F., Anjum, A., Peters, H., Dizon, R., Sayeeda, Z., Tian, S., Lee, B.L., Berjanskii, M., Mah, R., Yamamoto, M., Jovel, J., Torres-Calzada, C., Hiebert-Giesbrecht, M., Lui, V.W., Varshavi, D., Varshavi, D., Allen, D., Arndt, D., Khetarpal, N., Sivakumaran, A., Harford, K., Sanford, S., Yee, K., Cao, X., Budinski, Z., Liigand, J., Zhang, L., Zheng, J., Mandal, R., Karu, N., Dambrova, M.,

Schiöth, H.B., Greiner, R., Gautam, V., 2022. HMDB 5.0: the Human Metabolome Database for 2022. D622–D631 Nucleic Acids Res. 50. https://doi.org/10.1093/nar/gkab1062.

Wu, Y., Wang, X., Yang, L., Kang, S., Yan, G., Han, Y., Fang, H., Sun, H., 2023. Therapeutic Effects of Alisma orientale and its Active Constituents on Cardiovascular Disease and Obesity. Am. J. Chin. Med. 51, 623–650. https://doi.org/10.1142/S0192415X23500301.

Xia, F., Li, Y., Deng, L., Ren, R., Ge, B., Liao, Z., Xiang, S., Zhou, B., 2022. Alisol B 23-Acetate Ameliorates Lipopolysaccharide-Induced Intestinal Barrier Dysfunction by Inhibiting TLR4-NOX1/ROS Signaling Pathway in Caco-2 Cells. Front. Pharmacol. 13, 911196 https://doi.org/10.3389/fphar.2022.911196.

Xing, Y., Wang, X., Wang, X., Zhao, X., Guo, Y., Huang, Y., Teka, T., Han, L., Pan, G., 2023. The integrated analysis strategy of unstable hypoxanthine, a potential quality marker in Shuxuetong injection based on standard addition method and multi-level pharmacokinetics by LC-MS/MS. Acupuncture and Herbal Medicine 3, 116. https://doi.org/10.1097/HM9.0000000000000065.

Xue, L., Li, X., Zhu, X., Zhang, J., Zhou, S., Tang, W., Chen, D., Chen, Y., Dai, J., Wu, M., Wu, M., Wang, S., 2022. Carbon tetrachloride exposure induces ovarian damage through oxidative stress and inflammatory mediated ovarian fibrosis. Ecotoxicol. Environ. Saf. 242, 113859 https://doi.org/10.1016/j.ecoenv.2022.113859.

Yang, K., Zhang, J., Zhao, L., Cheng, L., Li, Y., Kang, Y., Zhang, X., Kang, Y., 2022. An umbrella review of Lianhua Qingwen combined with Western medicine for the treatment of coronavirus disease 2019. Acupuncture and Herbal Medicine 2, 143. https://doi.org/10.1097/HM9.0000000000000041.

Ye, M., Tang, Y., He, J., Cao, X., Liu, J., Kou, S., Yang, Y., Xue, J., Li, F., 2022. Alisol B 23-Acetate Increases the Antitumor Effect of Bufalin on Liver Cancer through Inactivating Wnt/β-Catenin Axis. Comput. Math. Methods Med. 2022, 6249534. https://doi.org/10.1155/2022/6249534.

Zahira, A., Sultana, S., Rasul, A., Sultana, T., Hassan, M., 2023. Hepatoprotective effects of almond shells against carbon tetrachloride induced liver injury in albino rats. Saudi J Biol Sci 30, 103811. https://doi.org/10.1016/j.sjbs.2023.103811.

Zhao, Y.-R., Dong, J.-B., Li, Y., Wu, M.-P., 2012. Sphingomyelin synthase 2 over-expression induces expression of aortic inflammatory biomarkers and decreases circulating EPCs in ApoE KO mice. Life Sci. 90, 867–873. https://doi.org/10.1016/j.lfs.2012.04.003.

Zheng, Y., Zhu, Y., Peng, G., 2006. Transformation of alisol B 23-acetate in processing of Alisma orientalis. Chin. Tradit. Herb. Drug 1479–1482.

Zheng, Y., Zhu, Y., Peng, G., 2015. Transformation of alisol B 23-acetate in processing of Alisma orientalis. Zhong Cao Yao 1479–1482.

Zhu, H.-C., Jia, X.-K., Fan, Y., Xu, S.-H., Li, X.-Y., Huang, M.-Q., Lan, M.-L., Xu, W., Wu, S.-S., 2021. Alisol B 23-Acetate Ameliorates Azoxymethane/Dextran Sodium Sulfate-Induced Male Murine Colitis-Associated Colorectal Cancer via Modulating the Composition of Gut Microbiota and Improving Intestinal Barrier. Front. Cell. Infect. Microbiol. 11, 640225 https://doi.org/10.3389/fcimb.2021.640225.